

Article

Cellulose Nanocrystals Induced Loose and Porous Graphite Phase Carbon Nitride/Porous Carbon Composites for Capturing and Determining of Organochlorine Pesticides from Water and Fruit Juice by Solid-Phase Microextraction

Huimin Li ¹, Panlong Dong ¹, Anying Long ^{2,*}, Suling Feng ¹, Jing Fan ¹ and Shengrui Xu ^{1,*} 

- ¹ Key Laboratory of Green Chemical Media and Reactions, Ministry of Education, Collaborative Innovation Center of Henan Province for Green Manufacturing of Fine Chemicals, School of Environment, School of Chemistry and Chemical Engineering, Henan Normal University, Xinxiang 453007, China; ming1391027849@163.com (H.L.); pldong2000@163.com (P.D.); slfeng@htu.cn (S.F.); fanjing@htu.cn (J.F.)
- ² 113 Geological Brigade, Bureau of Geology and Mineral Exploration and Development Guizhou Province, Liupanshui 553000, China
- * Correspondence: longying031042@163.com (A.L.); xushengrui@126.com (S.X.)

Abstract: Herein, novel, loose, and porous graphite phase carbon nitride/porous carbon (g-C₃N₄@PC) composites were prepared by decorating cellulose nanocrystals (CNCs). The characterization results demonstrate that the as-prepared composites presented high specific surface areas, porous structures, and abundant chemical groups, with the modification of CNCs. In view of the unique advantages, g-C₃N₄@PC was used as the coating material for the solid-phase microextraction (SPME) of organochlorine pesticides (OCPs) in water and juice samples. The g-C₃N₄@PC-coated fibers showed better extraction efficiencies than commercial fibers (100/7 μm PDMS and PA) toward the OCPs, with the enrichment factors of the g-C₃N₄@PC-coated fibers 5–30 times higher than the latter. Using a gas chromatography–mass spectrometry (GC-MS) instrument, the g-C₃N₄@PC-coated fibers exhibited a gratifying analytical performance for determining low concentrations of OCPs, with a wide linear range (0.1–1600 ng L⁻¹ for water; 0.1–1000 ng L⁻¹ for juice), low limits of detection (0.0141–0.0942 ng L⁻¹ for water; 0.0245–0.0777 ng L⁻¹ for juice), and good reproducibility and repeatability in optimal conditions. The established method showed good sensitivity and recovery in the determination of OCPs in the water and fruit juice samples, which displayed broad prospects for analyzing organic pollutants from environmental samples.

Keywords: cellulose nanocrystals; graphitized carbon nitride; organochlorine pesticides; solid-phase microextraction; gas chromatography–mass spectrometry



Citation: Li, H.; Dong, P.; Long, A.; Feng, S.; Fan, J.; Xu, S. Cellulose Nanocrystals Induced Loose and Porous Graphite Phase Carbon Nitride/Porous Carbon Composites for Capturing and Determining of Organochlorine Pesticides from Water and Fruit Juice by Solid-Phase Microextraction. *Polymers* **2023**, *15*, 2218. <https://doi.org/10.3390/polym15092218>

Academic Editor: Zhikun Zheng

Received: 22 March 2023

Revised: 30 April 2023

Accepted: 6 May 2023

Published: 8 May 2023



Copyright: © 2023 by the authors. Licensee MDPI, Basel, Switzerland. This article is an open access article distributed under the terms and conditions of the Creative Commons Attribution (CC BY) license (<https://creativecommons.org/licenses/by/4.0/>).

1. Introduction

In the 1950s, organochlorine pesticides (OCPs) became prevalent [1] and were mainly used in agricultural production, significantly boosting the demand for food supply. However, OCPs have a high persistence and biomagnification effect [2]. On the one hand, they can accumulate in organisms for prolonged periods, and on the other hand, they can form the effect of long-distance migration through soil and surface water [3], ultimately endangering human health, causing various serious harmful diseases, such as cancer [4,5], reproductive dysfunction, birth defects, immunotoxicity, and neurotoxicity [6–9]. This is highly detrimental to human health and global ecological sustainable development. Due to its excessive harm, the use of organochlorine was banned in 2004. Although these OCPs have been banned, they may still remain in water samples [10], soils [11], sediments [12], aquatic organisms [13], and human bodies [14,15] due to their high persistence. Therefore, there is an urgent need to establish a sensitive and accurate analytical method to monitor

OCP residues in the ecological environment, which is of great significance for human development.

In general, sample pretreatment is essential prior to the detection of OCPs using gas chromatography–mass spectrometry (GC-MS). Among various sample pretreatment techniques, solid-phase microextraction (SPME) attracted great interest owing to its unique advantages, such as solvent-free approach, high sensitivity, and straightforward operation [16–18]. Till now, SPME has been widely used in the analysis of environmental pollutants, food composition, drug content, biological components, etc. [19–24]. The extraction performance of SPME mainly depends on the coating materials, which determine the selectivity, sensitivity, and reproducibility of the analytical method [25–27]. Therefore, it is necessary to develop new SPME coating materials to meet diversified analysis for ultra-trace analytes.

As a new nonmetallic material, polymeric graphitized carbon nitride ($g\text{-C}_3\text{N}_4$) has attracted much attention owing to its advantages of a large specific surface area, excellent chemical and thermal stability, and low toxicity. Owing to these distinctive characteristics, $g\text{-C}_3\text{N}_4$ has been used as a new and efficient SPME coating material [28,29]. The two-dimensional nanosheet structure of $g\text{-C}_3\text{N}_4$ resembles that of graphene [30], and its layers are connected by conjugated π bonds formed by the sp^2 hybridization of carbon and nitrogen atoms, as well as weak van der Waals forces [31–33]. Due to the incomplete condensation of the triazine ring and the existence of the delocalized π bond, $g\text{-C}_3\text{N}_4$ contains rich nitrogen-containing functional groups, electron-rich properties, and crystal defects, which provide abundant adsorption active sites for targeted compounds [34]. However, $g\text{-C}_3\text{N}_4$ tends to agglomerate during the synthesis process of thermal polymerization, which seriously affects its properties and leads to the reduction of adsorption sites [35]. Therefore, to overcome these limitations of $g\text{-C}_3\text{N}_4$, it is necessary to introduce a template material as the support material.

Cellulose nanocrystals (CNCs) possess numerous oxygen-containing functional groups, such as hydroxyl, on their surface, which aid in the formation of intermolecular interactions. At the same time, the hydrogen bonds formed by intermolecular interaction are conducive to the construction of three-dimensional structures [36]. Furthermore, the surface of CNCs contains a high concentration of hydroxyl groups that can be easily chemically modified [37]. Leveraging these advantages, CNCs can be used as the support material for $g\text{-C}_3\text{N}_4$.

In this study, $g\text{-C}_3\text{N}_4$ was prepared by calcining urea in a muffle furnace. Subsequently, graphite phase carbon nitride/porous carbon ($g\text{-C}_3\text{N}_4\text{@PC}$) was synthesized with $g\text{-C}_3\text{N}_4$ as the precursor and CNCs as the support and was used as a new type of SPME coating. Notably, the newly obtained $g\text{-C}_3\text{N}_4\text{@PC}$ coating exhibited superior extraction capabilities compared to a pristine $g\text{-C}_3\text{N}_4$ coating and commercial coatings, which corresponded to its high surface area and abundant chemical groups. Finally, the proposed analytical method was successfully applied to the determination of trace OCPs in real environmental water and fruit juice samples.

2. Experimental

2.1. Reagents, Materials, and Instruments

The OCP standards, including etridiazole (ETR), chloroneb (CHE), trifluralin (TRI), hexachlorobenzene (HEX), chlorothalonil (CHT), chlorpyrifos (CHP), alpha-chlordane ($\alpha\text{-CHD}$), and gamma-chlordane ($\gamma\text{-CHD}$), were provided by AccuStandard Inc. (New Haven, CT, USA). Specific details of the reagents and instruments are clarified in Section S1.

2.2. Synthesis of $g\text{-C}_3\text{N}_4\text{@PC}$

Synthesis of $g\text{-C}_3\text{N}_4$: $g\text{-C}_3\text{N}_4$ was obtained using high-temperature treatment of urea according to the previous literature. Typically, 15 g urea was placed into a 100 mL crucible and sealed with aluminum foil. Then, the crucible was put into the muffle furnace, the

temperature was raised from 30 to 550 °C at a rate of 5 °C min⁻¹, and kept for 4 h. Finally, g-C₃N₄ powder was obtained after cooling to room temperature.

Synthesis of g-C₃N₄@PC: g-C₃N₄ powder and CNCs were dispersed in 20 mL of deionized water and subjected to ultrasonication for 2 h to form a suspension. Subsequently, the mixture was put into a freeze dryer and vacuum dried for 2 d to obtain g-C₃N₄/CNC aerogels. Then, these yellow aerogels were put into a tube furnace for pyrolysis under N₂ atmosphere. The temperature of the tubular furnace rose to 550 °C at a rate of 2 °C min⁻¹ and kept for 2 h. Finally, the g-C₃N₄@PC powder was obtained after cooling to room temperature, where the mass ratios of g-C₃N₄ and CNCs were set to 1:1, 2:1, 3:1, 1:2, and 1:3, which were labeled as g-C₃N₄@PC-1, g-C₃N₄@PC-2, g-C₃N₄@PC-3, g-C₃N₄@PC-4, and g-C₃N₄@PC-5, respectively.

2.3. Fabrication of g-C₃N₄@PC-Coated SPME Fibers

According to our previous studies [38,39], SPME fibers were fabricated using the adhesive method. Typically, a 3–4 cm long stainless steel wire was washed in nitric acid, sodium hydroxide, and anhydrous ethanol solutions, respectively, and then cleaned with deionized water. After drying, the stainless steel wire was coated evenly with g-C₃N₄@PC powder using silicone adhesive. Finally, the g-C₃N₄@PC SPME coating was obtained after drying at 130 °C in an oven. It is important to note that the newly acquired g-C₃N₄@PC SPME fiber needed to undergo heat treatment at the injection port of GC-MS for 20 min prior to use.

2.4. SPME Procedure and GC-MS Analysis

In the SPME process, 10 mL of sample solution was first added into 20 mL of vial. Subsequently, the as-prepared SPME fiber was inserted into the solution for extraction. During the extraction process, the temperature was controlled at 30–70 °C, extraction time was kept at 10–50 min, pH values ranged from 3 to 11, NaCl was used to control the ionic strength of solution from 0 to 30%, and all extraction experiments were repeated 3 times. Upon completion of the extraction, the SPME fiber made was instantly immersed into the GC-MS injection port for detection of the adsorbed substances on the coating. The details of GC-MS parameters and characteristic ion conditions for detecting OCPs are described in Tables S1 and S2.

2.5. Analysis of Real Water and Fruit Juice Samples

The real water samples originated from tap water (1#), Weihe River (2#), and rain water (3#), near Henan Normal University (Xinxiang, China). Fruit juice samples, including grape juice (4#), orange juice (5#), and peach juice (6#), which are popular beverages with the public, were purchased from local supermarkets in Xinxiang City, China. To remove any suspended solids and fine impurities from the fruit juice sample, it was centrifuged at 10,000 rpm for 20 min. After that, the resulting supernatant was filtered using a 0.45 µm filter membrane to remove macromolecular substances and minimize the effect of matrix substances. The filtered fruit juices were then diluted in deionized water to a certain proportion. Before analysis, both water and juice samples were stored in a refrigerator at 4 °C.

3. Results and Discussion

3.1. Characterizations of g-C₃N₄@PC Materials

The surface morphology and microstructure of the as-prepared g-C₃N₄@PC were determined using SEM and TEM (Figure 1). Figure 1a shows that g-C₃N₄ presented a disordered porous nanosheet structure. g-C₃N₄@PC-4 (Figure 1b) was a nanosheet structure composed of many stacked sheets with a diameter of about 100–200 nm, which showed that under the hydrogen bonding of CNCs, its interlayer connection was more tight, and its layered structure was more clear and irregular. In addition, the optical microscope image of the g-C₃N₄@PC-4 SPME fiber showed that the surface of the stainless steel wire

was evenly covered by g-C₃N₄@PC-4 composites (Figure 1c). The coating thickness was calculated as 64 μm based on the difference between the diameters of the fiber before and after coating, wherein the diameter of the stainless steel wire was 131 μm. Furthermore, TEM analysis (Figure 1d) shows the typical lamellar structure of g-C₃N₄. Figure 1e displays the decoration of the CNC-derived carbon fiber onto g-C₃N₄. Figure 1f further confirms the synthesis of g-C₃N₄@PC material with a lattice distance of 0.24 nm, which is consistent with the (100) crystal plane of the triazine ring unit [40,41].

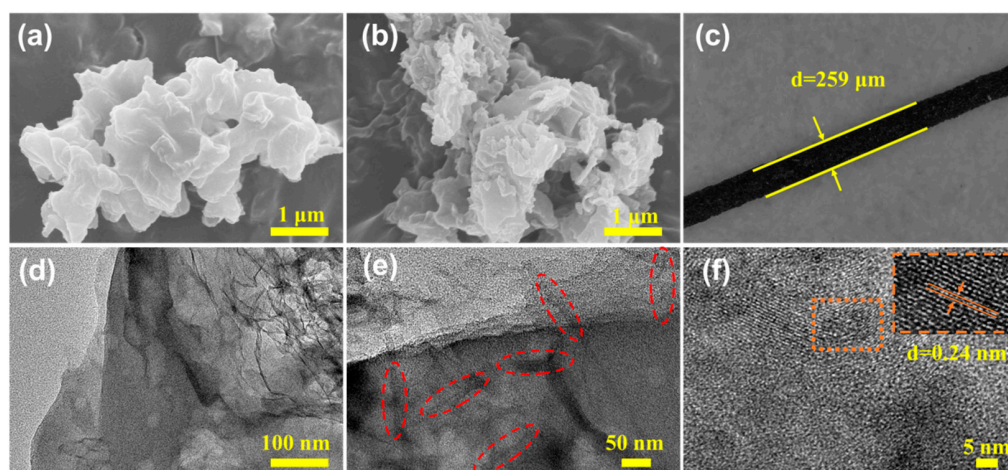


Figure 1. SEM images of (a) pure g-C₃N₄, (b) g-C₃N₄@PC-4, (c) optical microscope image of as-prepared g-C₃N₄@PC-4 SPME fiber and TEM images of (d) g-C₃N₄, (e,f) g-C₃N₄@PC-4, where, the CNC derived carbon fiber was highlighted with red dotted circle.

In order to survey the element composition and chemical state of the as-prepared g-C₃N₄ and g-C₃N₄@PC products, XPS analysis was performed in this study. Figure 2a displays three peaks referring to C 1s (295.63 eV), N 1s (410.63 eV), and O 1s (545.63 eV) both in g-C₃N₄ and g-C₃N₄@PC. The atomic contents of C, N, O were 55.61%, 42.48%, and 1.9% for g-C₃N₄ and 73.57%, 17.94%, and 8.49% for g-C₃N₄@PC-4, respectively. The high-resolution spectra of C 1s, N 1s, and O 1s are also shown in Figure 2b–d. For g-C₃N₄, it can be observed that the high-resolution spectra of C 1s owned three distinct peaks at 285.1, 288.2, and 288.7 eV, which referred to C–C, C=N, and N–C=N [42,43]. Compared with the g-C₃N₄ sample, a new peak was located at 285.8 eV, which corresponded to the C–O groups [44], indicating that the element C in g-C₃N₄@PC-4 was partially oxidized. In Figure 2c, the high-resolution N 1s spectra formed four peaks at 398.2, 399.1, 400.9, and 404.6 eV, which belonged to C–N=C, N–C₃, graphitic N and C–N–H, and –NH₂, respectively [45]. The O 1s spectra of g-C₃N₄ (Figure 2d) displayed two peaks at 532.5 and 533.2 eV, which can be regarded as C–OH and adsorbed O₂. Meanwhile, a new peak related to N–C–O was located at 531.8 eV in the O 1s spectrum of g-C₃N₄@PC-4 [46]. It is worth noting that the intensity of O 1s peak was significantly higher than that of g-C₃N₄, which demonstrated that more oxygen-containing functional groups were generated in g-C₃N₄@PC-4.

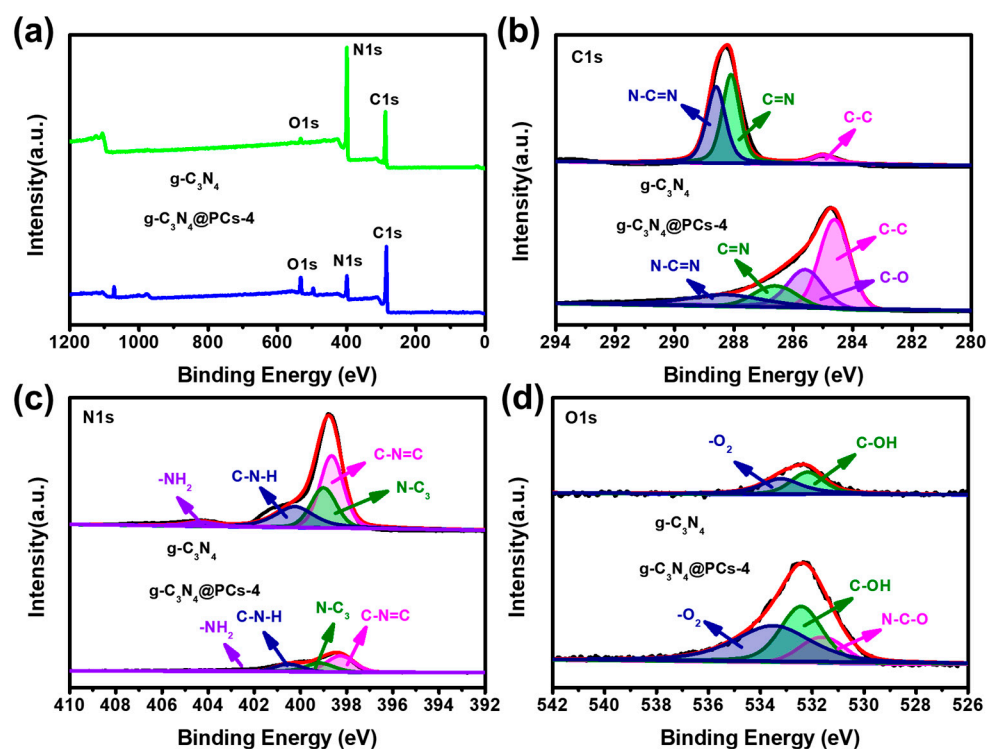


Figure 2. XPS survey spectrum (a) and high resolution XPS spectra of C 1s (b), N 1s (c), and O 1s (d) for $g\text{-C}_3\text{N}_4$ and $g\text{-C}_3\text{N}_4@\text{PC-4}$.

To verify the specific surface areas and pore size distributions of the prepared materials, N_2 adsorption/desorption isotherm curves and the BJH method were performed (Figure 3). The results show that the specific surface areas of $g\text{-C}_3\text{N}_4$, $g\text{-C}_3\text{N}_4@\text{PC-2}$, and $g\text{-C}_3\text{N}_4@\text{PC-4}$ were 51.1, 79.2, and 98.3 m^2/g , respectively. According to the BJH method (Figure 3b), the average pore sizes of $g\text{-C}_3\text{N}_4$, $g\text{-C}_3\text{N}_4@\text{PC-2}$, and $g\text{-C}_3\text{N}_4@\text{PC-4}$ were 85.7, 27.0, and 37.7 nm, respectively, indicating the formation of macroporous structures for $g\text{-C}_3\text{N}_4$ and mesoporous structures for $g\text{-C}_3\text{N}_4@\text{PC}$. At the same time, the pore volumes of $g\text{-C}_3\text{N}_4@\text{PC-4}$ presented a distinct increase to 0.9784 cm^3/g compared to pristine $g\text{-C}_3\text{N}_4$ (0.9145 cm^3/g). Abundant mesoporous structures and a higher specific surface area and pore capacity of $g\text{-C}_3\text{N}_4@\text{PC}$ compared to pristine $g\text{-C}_3\text{N}_4$ promoted the rapid diffusion of the target analytes and provided more adsorption active sites for the targeted analytes [47]. Moreover, TG was applied to investigate the thermal stability of the composites in this work. Figure 3c demonstrates that the as-prepared composites exhibited excellent thermal stability within 550 $^\circ\text{C}$.

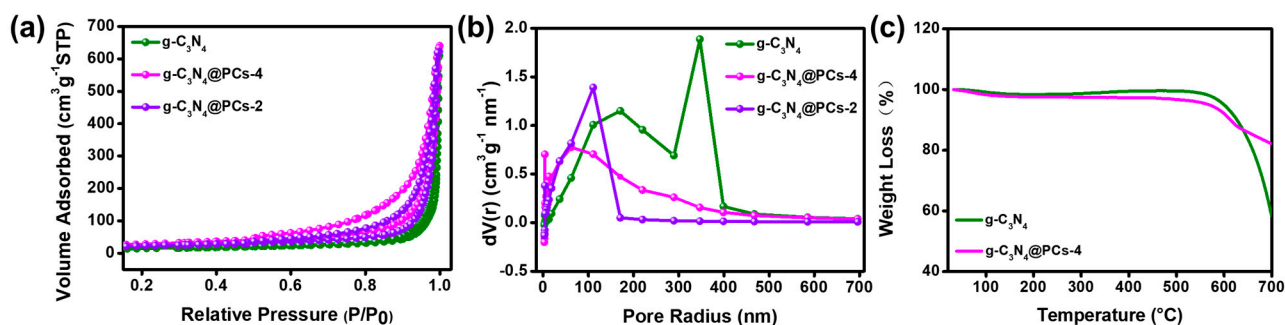


Figure 3. N_2 adsorption–desorption isotherm (a) and BJH pore size distribution (b) of as-prepared materials and thermal gravity analysis curve (c) of $g\text{-C}_3\text{N}_4$ and $g\text{-C}_3\text{N}_4@\text{PC-4}$.

3.2. Extraction Performance of $g\text{-C}_3\text{N}_4\text{@PC}$ -Coated SPME Fibers

To explore the extraction performances of the as-prepared composites, the extraction efficiencies of pristine $g\text{-C}_3\text{N}_4$ and $g\text{-C}_3\text{N}_4\text{@PC}$ toward OCPs were investigated by means of SPME. As shown in Figure 4a, the extraction efficiency of $g\text{-C}_3\text{N}_4\text{@PC}$ materials was significantly improved because of higher specific surface areas and richer chemical groups. As the enlargement of CNCs amounts, the extraction efficiencies of $g\text{-C}_3\text{N}_4\text{@PC}$ exhibited a trend of first increasing and then decreasing, and $g\text{-C}_3\text{N}_4\text{@PC-4}$ presented the optimum performance, owing to the synergy effects of $g\text{-C}_3\text{N}_4$ and CNCs. On the one hand, the introduction of CNCs promoted the formation of microporous and mesoporous structures, which increased the pore volume of $g\text{-C}_3\text{N}_4\text{@PC}$, resulting in an improvement in its adsorption capacity for target analytes. On the other hand, there were abundant oxygen-containing functional groups and other chemical groups in $g\text{-C}_3\text{N}_4\text{@PC}$, which promoted adsorption for polar groups. This is consistent with the results of the XPS characterization of $g\text{-C}_3\text{N}_4\text{@PC}$. However, when the amount of CNCs reached the maximum, the extraction efficiency decreased due to the reduction in intermolecular force and the influence of aggregates. Furthermore, comparisons of the extraction efficiencies between the $g\text{-C}_3\text{N}_4\text{@PC-4}$ coating and commercial PA and 7/100 μm PDMS were also studied (Figure 4b). It was found that the extraction efficiencies of $g\text{-C}_3\text{N}_4\text{@PC}$ SPME fibers for OCPs were much higher than that of PA and PDMS commercial coatings, with ratios approximately 5–30 and 2–15 times, respectively.

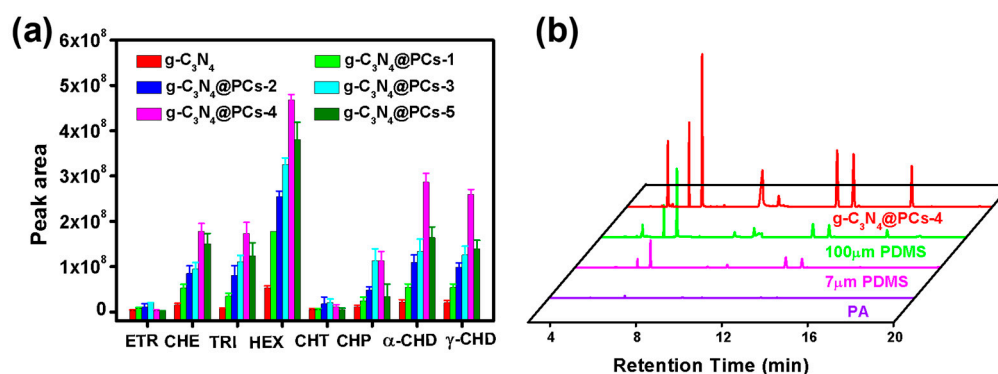


Figure 4. (a) Extraction capacities of $g\text{-C}_3\text{N}_4\text{@PC}$ with different ratios of $g\text{-C}_3\text{N}_4$ and CNCs and (b) GC-MS chromatograms of OCPs using $g\text{-C}_3\text{N}_4\text{@PC-4}$ and commercial fibers.

3.3. Optimization of $g\text{-C}_3\text{N}_4\text{@PC}$ -Coated SPME Conditions

Due to the change in extraction temperature, the distribution coefficient of analytes between the $g\text{-C}_3\text{N}_4\text{@PC}$ coating materials and the sample substrate changes and affects the mass and heat transfer effects of extraction efficiency. Increasing the extraction temperature makes for increasing the Henry constant and accelerating the entire extraction process. However, the distribution coefficient between the $g\text{-C}_3\text{N}_4\text{@PC}$ coating and the water sample showed a downward trend at this time, which reduces the extraction amount when the system is in equilibrium. Figure 5a displays the influence of temperature on the extraction performance of $g\text{-C}_3\text{N}_4\text{@PC}$ for OCPs. The extraction amount of OCPs showed a trend of first increasing and then decreasing as the temperature increased. The optimal extraction temperature for most analytes was 50 $^\circ\text{C}$ in this study.

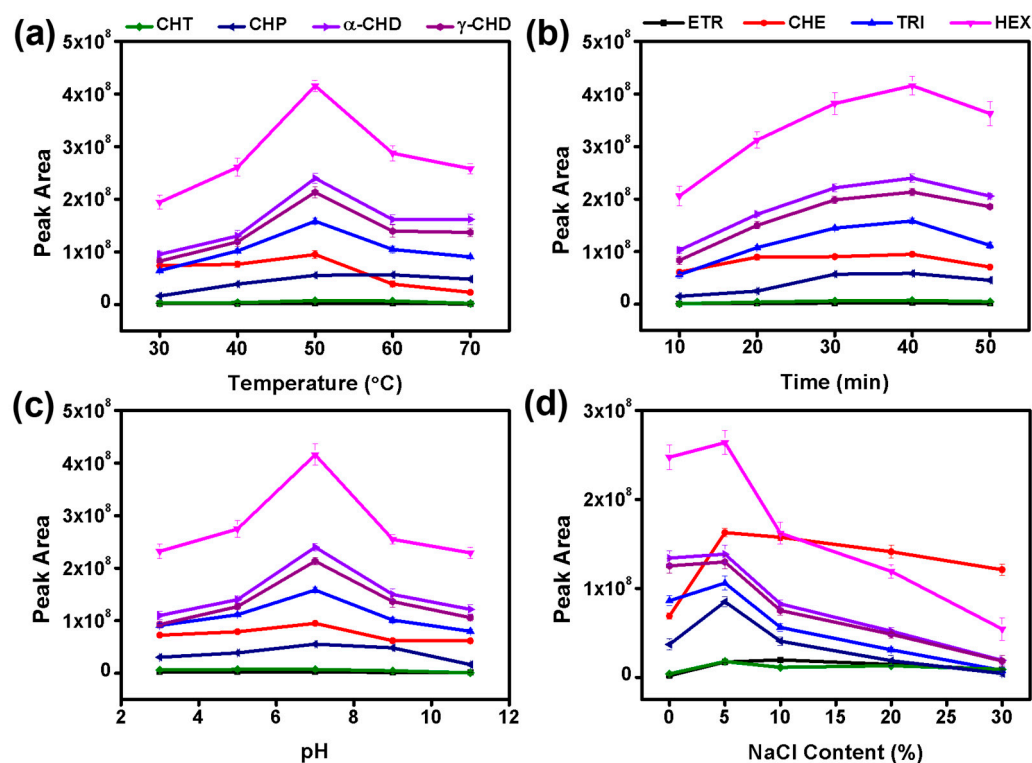


Figure 5. Effect of (a) extraction temperature, (b) extraction time, (c) pH, and (d) salt concentration on extraction efficiencies of $g\text{-C}_3\text{N}_4\text{@PC}$ SPME coating toward OCPs.

As SPME is a technology related to adsorption equilibrium, the effect of extraction time on extraction performance between 10 and 50 min was also investigated. In Figure 5b, the adsorption capacities for ETR, TRI, HEX, CHT, CHP, α -CHD, and γ -CHD increased with the extension of extraction time and approached the maximum adsorption equilibrium in 40 min. However, the absorption amounts for ETR, TRI, HEX, CHP, and α -CHD gradually showed signs of decreasing with the increase in extraction time, which was due to the potential competitive adsorption effect between OCPs and water [48,49]. In terms of both time consumption and extraction efficiency, the optimal extraction time for this work was set at 40 min.

The impact of solution pH was evaluated from 3 to 11, and the results show that the extraction efficiency reached its maximum at a pH of 7 (Figure 5c). Figure 5d shows the effect of NaCl on the extraction efficiency for OCPs. The results demonstrate that the extraction efficiency increased with a NaCl content of 5%, owing to the salting-out effect, whereas excessive NaCl content in solution reduced the extraction efficiency. This was due to the deposition of NaCl on the coating surface during the high-temperature desorption process in the GC-MS injector, which occupied the adsorption sites, resulting in a diminution in extraction efficiency for OCPs [50].

3.4. Method Validation and Real Sample Analysis

3.4.1. Validation of Proposed Analytical Method

Under the optimum conditions and parameters, $g\text{-C}_3\text{N}_4\text{@PC}$ SPME fibers were used to determine OCPs in water and fruit juice samples coupled with GC-MS. The performance parameters of this method included linear range, detection limit (LOD), limit of quantitation (LOQ), and precision (RSD). The results are listed in Tables 1 and 2. The proposed method had a linear range of $0.1\text{--}1600\text{ ng L}^{-1}$ for water samples with a correlation coefficient above 0.9913 and $0.1\text{--}1000\text{ ng L}^{-1}$ for the fruit juice samples. The LOD and LOQ were defined as a signal-to-noise ratio (S/N) of 3 and 10, respectively. The LOD and LOQ for eight OCPs in the water samples are $0.0141\text{--}0.0942\text{ ng L}^{-1}$ and $0.0471\text{--}0.3140\text{ ng L}^{-1}$; the LOD of the

fruit juice samples is 0.0245–0.0777 ng L⁻¹, and the LOQ is 0.0819–0.2591 ng L⁻¹. The RSD with a single fiber was 5.2–9.3% for water and 4.9–10.5% for fruit juice. The RSD with five fibers was 8.5–10.6% for water and 7.9–10.3% for fruit juice. The proposed method had a wide linear range, good reproducibility, and high sensitivity. To further demonstrate the superiority of the proposed method for determining OCPs, comparisons of the analytical method with other methods that are reported in the literature were investigated. As shown in Table 3, the proposed method presented higher sensitivity. Outstanding performances enabled the proposed method to be successfully applied to the analysis of OCPs in real water and fruit juice samples. Furthermore, we evaluated the reusability of the g-C₃N₄@PC SPME coating for determining OCPs. The results (Figure 6) show that there are no distinct changes in extraction efficiency within 200 times of reuse, indicating that the fibers had good durability.

Table 1. Extraction capacities of g-C₃N₄@PC SPME fibers toward OCPs from water.

Analytes	Linear Ranges (ng L ⁻¹)	R ²	LOD (ng L ⁻¹)	LOQ (ng L ⁻¹)	RSD (%)	
					One Fiber (n = 7)	Fiber-to-Fiber (n = 5)
ETR	0.1–1600	0.9995	0.0224	0.0749	5.2	8.9
CHN	0.1–1600	0.9960	0.0942	0.3140	7.3	9.2
TRI	0.1–1600	0.9913	0.0706	0.2355	6.4	8.5
HCB	0.1–1600	0.9972	0.0565	0.1884	8.9	10.7
CHT	0.1–1600	0.9978	0.0668	0.2228	7.6	9.4
CHP	0.1–1600	0.9960	0.0141	0.0471	9.3	9.7
α-CHD	0.1–1600	0.9933	0.0471	0.1570	6.5	10.1
γ-CHD	0.1–1600	0.9917	0.0565	0.1884	5.7	10.6

Table 2. Analytical performance of g-C₃N₄@PC SPME fibers toward OCPs from fruit juices.

Analytes	Linear Ranges (ng L ⁻¹)	R ²	LOD (ng L ⁻¹)	LOQ (ng L ⁻¹)	RSD (%)	
					One Fiber (n = 7)	Fiber-to-Fiber (n = 5)
ETR	0.1–1000	0.9924	0.0777	0.2591	4.9	7.9
CHN	0.1–500	0.9930	0.0282	0.0942	7.6	8.2
TRI	0.1–500	0.9904	0.0403	0.1345	5.4	9.5
HCB	0.1–500	0.9929	0.0256	0.0856	7.8	8.7
CHT	0.1–1000	0.9982	0.0565	0.1884	8.4	9.6
CHP	0.1–1000	0.9994	0.0314	0.1046	9.6	8.7
α-CHD	0.1–1000	0.9993	0.0245	0.0819	10.5	10.3
γ-CHD	0.1–1000	0.9967	0.0282	0.0941	6.7	10.1

Table 3. The comparison of methods for determination of OCPs in water.

Analytical Methods	Coating Materials	Linear Ranges (ng L ⁻¹)	LOD (ng L ⁻¹)	LOQ (ng L ⁻¹)	Reference
SPME/GC-MS	mesoporous TiO ₂	5–5000	0.08–0.60	0.27–2.00	[50]
HS-SPME/GC-ECD	porous aromatic framework/ionic liquid	1000–500,000	110–290	350–930	[51]
SPME/GC-MS	sol-gel-graphene	10–100,000	0.19–18.30	–	[52]
HS-SPME/GC-MS	DVB/CAR/PDMS	20–100,000	20–230	20–770	[53]
SPE/GC-ECD	Au/Ti-UVM-7	400–100,000	0.30–20	1–61	[54]
SPME/GC-ECD	AuNPs	560–10,000	130–240	440–810	[55]
SPME/GC-MS	carbonized polydopamine	10–50,000	1.40–15	–	[56]
SPME/GC-MS	C ₁₈ composite	2–500	0.059–0.151	–	[57]
SPME/GC-MS	g-C ₃ N ₄ @PC	0.1–1600	0.0141–0.0942	0.0471–0.3140	This work

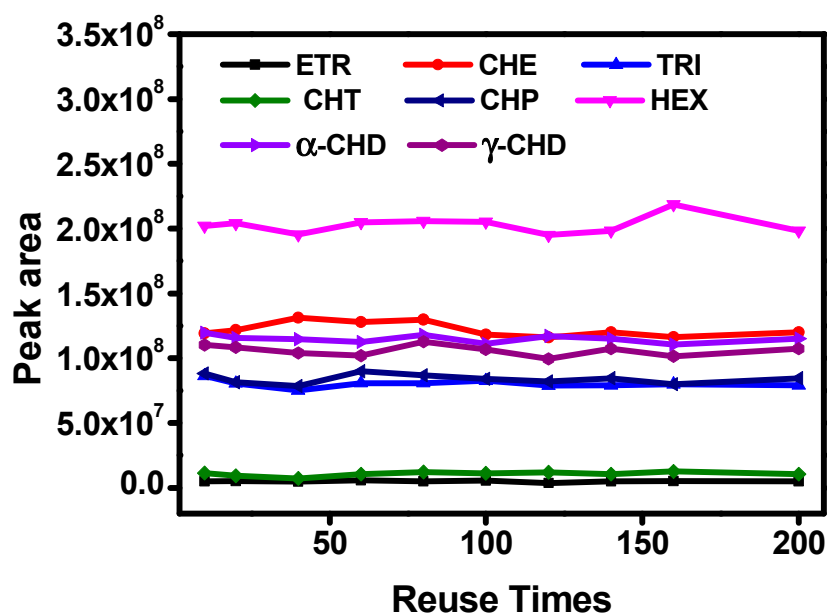


Figure 6. Reusability of g-C₃N₄@PC SPME coating toward OCPs.

3.4.2. Analysis of Real Water and Fruit Juice Samples

The OCPs in real water samples and fruit juice samples were analyzed using the proposed method. As shown in Tables 4 and 5, no OCP analytes were found in the tap water (1#), Weihe River (2#), grape juice (4#), and orange juice samples (5#). When the spiked concentration was 2 ng L⁻¹, the recovery rate of sample 1# was 93.2–125.5%, the standard recovery rate of sample 2# was 90.6–101.2%, and the recovery rate of sample 3# was 91.4–107.3%. Grape juice (4#) and orange juice (5#) were labeled with 1 ng L⁻¹; the recovery rate of sample 4# was 92.3–119.5%, and the recoveries of sample 5# were satisfied with a range of 92.7–113.8%. Peach juice (6#) was labeled with 0.1 ng L⁻¹, and the recovery rate of sample 6# was 93.9–106.3%. In summary, the established method of combining the coating material with a GC-MS instrument obtained a satisfactory recovery rate for determining OCPs both in water and fruit juice samples.

Table 4. Analytical results and recoveries for determination of OCPs from real water samples.

Analytes	Tap Water (1#)			Weihe River (2#)			Rain Water (3#)		
	Found (ng L ⁻¹)	RSD (% , n = 3)	Recoveries (% , Spiked with 2 ng L ⁻¹)	Found (ng L ⁻¹)	RSD (% , n = 3)	Recoveries (% , Spiked with 2 ng L ⁻¹)	Found (ng L ⁻¹)	RSD (% , n = 3)	Recoveries (% , Spiked with 0.2 ng L ⁻¹)
ETR	ND	–	125.5	ND	–	94.1	ND	–	93.5
CHN	ND	–	104.8	ND	–	93.4	ND	–	107.3
TRI	ND	–	96.4	ND	–	90.6	10.9	–	94.1
HCB	ND	–	122.4	ND	–	93.9	ND	–	95.7
CHT	ND	–	103.3	ND	–	101.2	ND	–	98.8
CHP	ND	–	93.2	ND	–	95.4	ND	–	93.3
α-CHD	ND	–	98.1	ND	–	98.3	ND	–	102.7
γ-CHD	ND	–	95.6	ND	–	97.6	ND	–	91.4

ND represents not detected.

Table 5. Analytical results and recoveries for determination of OCPs from fruit juice samples.

Analytes	Grape Juice(4#)			Orange Juice(5#)			Peach Juice(6#)		
	Found (ng L ⁻¹)	RSD (% , n = 3)	Recoveries (% , Spiked with 1 ng L ⁻¹)	Found (ng L ⁻¹)	RSD (% , n = 3)	Recoveries (% , Spiked with 1 ng L ⁻¹)	Found (ng L ⁻¹)	RSD (% , n = 3)	Recoveries (% , Spiked with 0.1 ng L ⁻¹)
ETR	ND	–	92.3	ND	–	92.7	ND	–	96.8
CHN	ND	–	94.4	ND	–	95.2	ND	–	97.2
TRI	ND	–	97.3	ND	–	98.2	10.9	–	95.6
HCB	ND	–	94.8	ND	–	95.6	ND	–	106.3
CHT	ND	–	107.9	ND	–	113.8	ND	–	98.2
CHP	ND	–	119.5	ND	–	94.3	ND	–	93.9
α-CHD	ND	–	95.8	ND	–	92.6	ND	–	96.1
γ-CHD	ND	–	98.7	ND	–	108.3	ND	–	95.5

ND represents not detected.

4. Conclusions

In this study, a novel g-C₃N₄@PC composite was synthesized using CNCs as the support. In view of its outstanding advantages of a high specific surface area, porous structure, and abundant chemical groups, the g-C₃N₄@PC composite was used as an SPME coating for extracting OCPs. The mesoporous channels in g-C₃N₄@PC were helpful to enhance the mass transfer rate of the analytes. In addition, the addition of CNCs made g-C₃N₄ have a rich pore structure, providing more active sites for the adsorption and transportation of analytes; therefore, the g-C₃N₄@PC-coated fiber exhibited higher extraction efficiency for OCPs than pristine g-C₃N₄ and commercial SPME coatings. The established method was successfully applied to the analysis of OCPs in environmental water samples and fruit juice samples. This study proposed a novel SPME coating material for capturing and determining trace organic pollutants from environmental media and food samples.

Supplementary Materials: The following supporting information can be downloaded at: <https://www.mdpi.com/article/10.3390/polym15092218/s1>, Section S1: Apparatus used for characterization of materials; Table S1: Operating parameters of GC–MS; Table S2: Retention time and characteristic ions of OCPs.

Author Contributions: H.L.: investigation and writing—original draft preparation; P.D.: validation and formal analysis; A.L.: conceptualization, methodology, and funding acquisition; S.F.: project administration; J.F.: resources; S.X.: writing—review and editing, conceptualization, and supervision. All authors have read and agreed to the published version of the manuscript.

Funding: This work was financially supported by funding from the National Natural Science Foundation of China (21976052), Natural Science Foundation of Guizhou Province of China ([2019]1423), and the Foundation of Bureau of Geology and Mineral Exploration and Development Guizhou Province ([2019]16).

Institutional Review Board Statement: Not applicable.

Data Availability Statement: This study presents novel concepts and did not report any data.

Acknowledgments: The authors would like to thank Yuxiang Wu from Shiyanjia Lab (www.shiyanjia.com) for the BET analysis accessed on 31 December 2021.

Conflicts of Interest: The authors declare no conflict of interest.

References

- Braune, B.M.; Outridge, P.M.; Fisk, A.T.; Muir, D.C.; Helm, P.A.; Hobbs, K.; Hoekstra, P.F.; Kuzyk, Z.A.; Kwan, M.; Letcher, R.J.; et al. Persistent organic pollutants and mercury in marine biota of the Canadian Arctic: An overview of spatial and temporal trends. *Sci. Total Environ.* **2005**, *351–352*, 4–56. [[CrossRef](#)] [[PubMed](#)]
- Qiu, J.; Chen, G.; Xu, J.; Luo, E.; Liu, Y.; Wang, F.; Zhou, H.; Liu, Y.; Zhu, F.; Ouyang, G. In vivo tracing of organochloride and organophosphorus pesticides in different organs of hydroponically grown malabar spinach (*Basella alba* L.). *J. Hazard. Mater.* **2016**, *316*, 52–59. [[CrossRef](#)] [[PubMed](#)]

3. Lupi, L.; Bedmar, F.; Wunderlin, D.A.; Miglioranza, K.S.B. Levels of organochlorine pesticides in soils, mesofauna and streamwater from an agricultural watershed in Argentina. *Environ. Earth Sci.* **2019**, *78*, 569. [[CrossRef](#)]
4. Guida, Y.; Carvalho, G.O.; Capella, R.; Pozo, K.; Lino, A.S.; Azeredo, A.; Carvalho, D.F.P.; Braga, A.L.F.; Torres, J.P.M.; Meire, R.O. Atmospheric Occurrence of Organochlorine Pesticides and Inhalation Cancer Risk in Urban Areas at Southeast Brazil. *Environ. Pollut.* **2021**, *271*, 116359. [[CrossRef](#)] [[PubMed](#)]
5. Attaullah, M.; Yousuf, M.J.; Shaikat, S.; Anjum, S.I.; Ansari, M.J.; Buner, I.D.; Tahir, M.; Amin, M.; Ahmad, N.; Khan, S.U. Serum organochlorine pesticides residues and risk of cancer: A case-control study. *Saudi J. Biol. Sci.* **2018**, *25*, 1284–1290. [[CrossRef](#)]
6. Lin, B.G.; Chen, C.R.; Chen, X.C.; Qiao, J.; Yan, Q.X.; Yang, P.; Chen, W.L.; Li, L.Z.; Qiu, P.C.; Ding, C.; et al. Effects of organochlorine exposure on male reproductive disorders in an electronic waste area of South China. *Environ. Int.* **2021**, *147*, 106318. [[CrossRef](#)]
7. Nicolopoulou-Stamati, P.; Maipas, S.; Kotampasi, C.; Stamatis, P.; Hens, L. Chemical Pesticides and Human Health: The Urgent Need for a New Concept in Agriculture. *Front. Public Health* **2016**, *4*, 148. [[CrossRef](#)]
8. Sawyna, J.M.; Spivia, W.R.; Radecki, K.; Fraser, D.A.; Lowe, C.G. Association between chronic organochlorine exposure and immunotoxicity in the round stingray (*Urobatis halleri*). *Environ. Pollut.* **2017**, *223*, 42–50. [[CrossRef](#)]
9. Choi, S.; Kim, H.J.; Kim, S.; Choi, G.; Kim, S.; Park, J.; Shim, S.S.; Lee, I.; Kim, S.; Moon, H.B.; et al. Current status of organochlorine pesticides (OCPs) and polychlorinated biphenyls (PCBs) exposure among mothers and their babies of Korea-CHECK cohort study. *Sci. Total Environ.* **2018**, *618*, 674–681. [[CrossRef](#)]
10. Liu, J.; Qi, S.; Yao, J.; Yang, D.; Xing, X.; Liu, H.; Qu, C. Contamination characteristics of organochlorine pesticides in multimatrix sampling of the Hanjiang River Basin, southeast China. *Chemosphere* **2016**, *163*, 35–43. [[CrossRef](#)]
11. Lupi, L.; Bedmar, F.; Wunderlin, D.A.; Miglioranza, K.S.B. Organochlorine pesticides in agricultural soils and associated biota. *Environ. Earth Sci.* **2016**, *75*, 519. [[CrossRef](#)]
12. Jin, M.; Fu, J.; Xue, B.; Zhou, S.; Zhang, L.; Li, A. Distribution and enantiomeric profiles of organochlorine pesticides in surface sediments from the Bering Sea, Chukchi Sea and adjacent Arctic areas. *Environ. Pollut.* **2017**, *222*, 109–117. [[CrossRef](#)]
13. Islam, M.M.; Avha, N.J.; Ahmed, S.; Akbor, M.A.; Islam, M.S.; Mostafiz, F.; Habibullah-Al-Mamun, M. Trace metals and organochlorine pesticide residues in imported fishes in Bangladesh and human health risk implications. *Environ. Sci. Pollut. R.* **2022**, *29*, 17499–17512. [[CrossRef](#)] [[PubMed](#)]
14. Thomas, A.; Toms, L.L.; Harden, F.A.; Hobson, P.; White, N.M.; Mengersen, K.L.; Mueller, J.F. Concentrations of organochlorine pesticides in pooled human serum by age and gender. *Environ. Res.* **2017**, *154*, 10–18. [[CrossRef](#)]
15. Pastor Belda, M.; Gonzalez-Franco, J.A.; Rubio, R.; Campillo, N.; Hernandez-Cordoba, M.; Torres, C.; Perez-Carceles, M.D.; Vinas, P. Occurrence of Organochlorine Pesticides in Human Tissues Assessed Using a Microextraction Procedure and Gas Chromatography-Mass Spectrometry. *J. Anal. Toxicol.* **2021**, *45*, 84–92. [[CrossRef](#)]
16. Zhang, Q.; Zhou, L.; Chen, H.; Wang, C.; Xia, Z.; Yuan, C. Solid-phase microextraction technology for in vitro and in vivo metabolite analysis. *TrAC Trend. Anal. Chem.* **2016**, *80*, 57–65. [[CrossRef](#)] [[PubMed](#)]
17. Billiard, K.; Dershem, A.; Gionfriddo, E. Implementing Green Analytical Methodologies Using Solid-Phase Microextraction: A Review. *Molecules* **2020**, *25*, 5297. [[CrossRef](#)] [[PubMed](#)]
18. Onat, B.; Rosales-Solano, H.; Pawliszyn, J. Development of a Biocompatible Solid Phase Microextraction Thin Film Coating for the Sampling and Enrichment of Peptides. *Anal. Chem.* **2020**, *92*, 9379–9388. [[CrossRef](#)]
19. Xu, S.; Liu, H.; Long, A.; Feng, S.; Chen, C.-P. In-situ synthesis of carbon dots embedded wrinkled-mesoporous silica microspheres for efficiently capturing and monitoring organochlorine pesticides from water and fruit juice. *Sep. Purif. Technol.* **2023**, *306*, 122589. [[CrossRef](#)]
20. Xu, S.; Liu, H.; Chen, C.; Feng, S.; Fan, J. Ultrasound-assisted one-step reduction and self-assembly of carbon dots-reduced graphene oxide: Mechanism investigation and solid phase microextraction of ultra-trace organochlorine pesticides. *Chem. Eng. J.* **2023**, *451*, 138569. [[CrossRef](#)]
21. Wang, M.; Wu, H.; Xu, S.; Dong, P.; Long, A.; Xiao, L.; Feng, S.; Chen, C. Cellulose nanocrystal regulated ultra-loose, lightweight, and hierarchical porous reduced graphene oxide hybrid aerogel for capturing and determining organic pollutants from water. *Carbon* **2023**, *204*, 94–101. [[CrossRef](#)]
22. Queiroz, M.E.C.; Souza, I.D.d.; Oliveira, I.G.d.; Grecco, C.F. In vivo solid phase microextraction for bioanalysis. *TrAC Trend. Anal. Chem.* **2022**, *153*, 116656. [[CrossRef](#)]
23. Xu, S.; Li, H.; Wu, H.; Xiao, L.; Dong, P.; Feng, S.; Fan, J. A facile cooling-assisted solid-phase microextraction device for solvent-free sampling of polycyclic aromatic hydrocarbons from soil based on matrix solid-phase dispersion technique. *Anal. Chim. Acta* **2020**, *1115*, 7–15. [[CrossRef](#)]
24. Llompart, M.; Celeiro, M.; Garcia-Jares, C.; Dagnac, T. Environmental applications of solid-phase microextraction. *TrAC Trend. Anal. Chem.* **2019**, *112*, 1–12. [[CrossRef](#)]
25. Li, J.; Wang, Z.; Li, J.; Zhang, S.; An, Y.; Hao, L.; Yang, X.; Wang, C.; Wang, Z.; Wu, Q. Novel N-riched covalent organic framework for solid-phase microextraction of organochlorine pesticides in vegetable and fruit samples. *Food Chem.* **2022**, *388*, 133007. [[CrossRef](#)]
26. Liu, Y.; Huang, Y.; Chen, G.; Huang, J.; Zheng, J.; Xu, J.; Liu, S.; Qiu, J.; Yin, L.; Ruan, W.; et al. A graphene oxide-based polymer composite coating for highly-efficient solid phase microextraction of phenols. *Anal. Chim. Acta* **2018**, *1015*, 20–26. [[CrossRef](#)] [[PubMed](#)]

27. Zhang, N.; Lei, X.; Huang, T.; Su, L.; Zhang, L.; Xie, Z.; Wu, X. Guanidyl-functionalized polyhedral oligomeric silsesquioxane porous hybrid polymer coating for specific solid phase microextraction of phthalate esters in foodstuff. *Chem. Eng. J.* **2020**, *386*, 124003. [[CrossRef](#)]
28. Zhang, N.; Gao, J.; Huang, C.; Liu, W.; Tong, P.; Zhang, L. In situ hydrothermal growth of ZnO/g-C₃N₄ nanoflowers coated solid-phase microextraction fibers coupled with GC-MS for determination of pesticides residues. *Anal. Chim. Acta* **2016**, *934*, 122–131. [[CrossRef](#)]
29. Pang, Y.; Zang, X.; Li, H.; Liu, J.; Chang, Q.; Zhang, S.; Wang, C.; Wang, Z. Solid-phase microextraction of organophosphorous pesticides from food samples with a nitrogen-doped porous carbon derived from g-C₃N₄ templated MOF as the fiber coating. *J. Hazard. Mater.* **2020**, *384*, 121430. [[CrossRef](#)]
30. Sun, Y.P.; Chen, J.; Qi, H.Y.; Shi, Y.P. Graphitic carbon nitrides modified hollow fiber solid phase microextraction for extraction and determination of uric acid in urine and serum coupled with gas chromatography-mass spectrometry. *J. Chromatogr. B Analyt. Technol. Biomed. Life Sci.* **2015**, *1004*, 53–59. [[CrossRef](#)]
31. Ashritha, M.G.; Hareesh, K. A review on Graphitic Carbon Nitride based binary nanocomposites as supercapacitors. *J. Energy Storage* **2020**, *32*, 101840. [[CrossRef](#)]
32. Fu, J.; Yu, J.; Jiang, C.; Cheng, B. g-C₃N₄ Based Heterostructured Photocatalysts. *Adv. Energy Mater.* **2018**, *8*, 1701503. [[CrossRef](#)]
33. Wu, T.; Wang, J.; Liang, W.; Zang, X.; Wang, C.; Wu, Q.; Wang, Z. Single layer graphitic carbon nitride-modified graphene composite as a fiber coating for solid-phase microextraction of polycyclic aromatic hydrocarbons. *Microchim. Acta* **2017**, *184*, 2171–2180. [[CrossRef](#)]
34. Yang, Y.; Qin, P.; Zhang, X.; Niu, J.; Tian, S.; Lu, M.; Zhu, J.; Cai, Z. Layer-by-layer fabrication of g-C₃N₄ coating for headspace solid-phase microextraction of food additives followed by gas chromatography-flame ionization detection. *Anal. Methods* **2018**, *10*, 322–329. [[CrossRef](#)]
35. Yang, Y.; Qin, P.; Zhang, J.; Li, W.; Zhu, J.; Lu, M.; Cai, Z. Fabrication of nanoscale graphitic carbon nitride/copper oxide hybrid composites coated solid-phase microextraction fibers coupled with gas chromatography for determination of polycyclic aromatic hydrocarbons. *J. Chromatogr. A* **2018**, *1570*, 47–55. [[CrossRef](#)]
36. Huang, F.; Lv, J.; Li, H.; Xu, S. Regulation rule of cellulose nanocrystals on thixotropy of hydrogel for water shutoff in horizontal wells. *Colloids Surf. A* **2022**, *643*, 128735. [[CrossRef](#)]
37. Georgouvelas, D.; Abdelhamid, H.N.; Li, J.; Edlund, U.; Mathew, A.P. All-cellulose functional membranes for water treatment: Adsorption of metal ions and catalytic decolorization of dyes. *Carbohydr. Polym.* **2021**, *264*, 118044. [[CrossRef](#)]
38. Xu, S.; Dong, P.; Liu, H.; Li, H.; Chen, C.; Feng, S.; Fan, J. Lotus-like Ni@NiO nanoparticles embedded porous carbon derived from MOF-74/cellulose nanocrystal hybrids as solid phase microextraction coating for ultrasensitive determination of chlorobenzenes from water. *J. Hazard. Mater.* **2022**, *429*, 128384. [[CrossRef](#)]
39. Xu, S.; Liu, H.; Long, A.; Li, H.; Chen, C.; Feng, S.; Fan, J. Carbon Dot-Decorated Graphite Carbon Nitride Composites for Enhanced Solid-Phase Microextraction of Chlorobenzenes from Water. *Nanomaterials* **2022**, *12*, 335. [[CrossRef](#)]
40. Chen, X.; Shi, R.; Chen, Q.; Zhang, Z.; Jiang, W.; Zhu, Y.; Zhang, T. Three-dimensional porous g-C₃N₄ for highly efficient photocatalytic overall water splitting. *Nano Energy* **2019**, *59*, 644–650. [[CrossRef](#)]
41. Chen, X.; Wang, J.; Chai, Y.; Zhang, Z.; Zhu, Y. Efficient Photocatalytic Overall Water Splitting Induced by the Giant Internal Electric Field of a g-C₃N₄/rGO/PDIP Z-Scheme Heterojunction. *Adv. Mater.* **2021**, *33*, 2007479. [[CrossRef](#)] [[PubMed](#)]
42. Wang, L.; Ding, J.; Chai, Y.; Liu, Q.; Ren, J.; Liu, X.; Dai, W.L. CeO₂ nanorod/g-C₃N₄/N-rGO composite: Enhanced visible-light-driven photocatalytic performance and the role of N-rGO as electronic transfer media. *Dalton Trans.* **2015**, *44*, 11223–11234. [[CrossRef](#)] [[PubMed](#)]
43. Ong, W.J.; Tan, L.L.; Chai, S.P.; Yong, S.T. Graphene oxide as a structure-directing agent for the two-dimensional interface engineering of sandwich-like graphene-g-C₃N₄ hybrid nanostructures with enhanced visible-light photoreduction of CO₂ to methane. *Chem. Commun.* **2015**, *51*, 858–861. [[CrossRef](#)] [[PubMed](#)]
44. Hou, Y.; Wen, Z.; Cui, S.; Guo, X.; Chen, J. Constructing 2D porous graphitic C₃N₄ nanosheets/nitrogen-doped graphene/layered MoS₂ ternary nanojunction with enhanced photoelectrochemical activity. *Adv. Mater.* **2013**, *25*, 6291–6297. [[CrossRef](#)]
45. Wang, Y.; Xia, Q.; Bai, X.; Ge, Z.; Yang, Q.; Yin, C.; Kang, S.; Dong, M.; Li, X. Carbothermal activation synthesis of 3D porous g-C₃N₄/carbon nanosheets composite with superior performance for CO₂ photoreduction. *Appl. Catal. B* **2018**, *239*, 196–203. [[CrossRef](#)]
46. Li, J.; Shen, B.; Hong, Z.; Lin, B.; Gao, B.; Chen, Y. A facile approach to synthesize novel oxygen-doped g-C₃N₄ with superior visible-light photoreactivity. *Chem. Commun.* **2012**, *48*, 12017–12019. [[CrossRef](#)]
47. Wu, H.; Li, C.; Che, H.; Hu, H.; Hu, W.; Liu, C.; Ai, J.; Dong, H. Decoration of mesoporous Co₃O₄ nanospheres assembled by monocrystal nanodots on g-C₃N₄ to construct Z-scheme system for improving photocatalytic performance. *Appl. Surf. Sci.* **2018**, *440*, 308–319. [[CrossRef](#)]
48. Gong, X.; Xu, L.; Huang, S.; Kou, X.; Lin, S.; Chen, G.; Ouyang, G. Application of the NU-1000 coated SPME fiber on analysis of trace organochlorine pesticides in water. *Anal. Chim. Acta* **2022**, *1218*, 339982. [[CrossRef](#)]
49. Wang, F.; Liu, S.; Yang, H.; Zheng, J.; Qiu, J.; Xu, J.; Tong, Y.; Zhu, F.; Ouyang, G. Hierarchical Graphene coating for highly sensitive solid phase microextraction of organochlorine pesticides. *Talanta* **2016**, *160*, 217–224. [[CrossRef](#)]
50. Liu, S.; Xie, L.; Zheng, J.; Jiang, R.; Zhu, F.; Luan, T.; Ouyang, G. Mesoporous TiO₂ nanoparticles for highly sensitive solid-phase microextraction of organochlorine pesticides. *Anal. Chim. Acta* **2015**, *878*, 109–117. [[CrossRef](#)]

51. Ke, Y.; Zhu, F.; Zeng, F.; Luan, T.; Su, C.; Ouyang, G. Preparation of graphene-coated solid-phase microextraction fiber and its application on organochlorine pesticides determination. *J. Chromatogr. A* **2013**, *1300*, 187–192. [[CrossRef](#)] [[PubMed](#)]
52. Wu, M.; Chen, G.; Liu, P.; Zhou, W.; Jia, Q. Preparation of porous aromatic framework/ionic liquid hybrid composite coated solid-phase microextraction fibers and their application in the determination of organochlorine pesticides combined with GC-ECD detection. *Analyst* **2016**, *141*, 243–250. [[CrossRef](#)] [[PubMed](#)]
53. Merib, J.; Simão, V.; Dias, A.N.; Carasek, E. Simultaneous determination of trihalomethanes and organochlorine pesticides in water samples by direct immersion-headspace-solid phase microextraction. *J. Chromatogr. A* **2013**, *1321*, 30–37. [[CrossRef](#)] [[PubMed](#)]
54. Pellicer-Castell, E.; Belenguer-Sapiña, C.; Amorós, P.; El Haskouri, J.; Herrero-Martínez, J.M.; Mauri-Aucejo, A.R. Mesoporous silica sorbent with gold nanoparticles for solid-phase extraction of organochlorine pesticides in water samples. *J. Chromatogr. A* **2022**, *1662*, 462729. [[CrossRef](#)] [[PubMed](#)]
55. Gutiérrez-Serpa, A.; Rocío-Bautista, P.; Pino, V.; Jiménez-Moreno, F.; Jiménez-Abizanda, A.I. Gold nanoparticles based solid-phase microextraction coatings for determining organochlorine pesticides in aqueous environmental samples. *J. Sep. Sci.* **2017**, *40*, 2009–2021. [[CrossRef](#)]
56. Huang, Z.; Chua, P.E.; Lee, H.K. Carbonized polydopamine as coating for solid-phase microextraction of organochlorine pesticides. *J. Chromatogr. A* **2015**, *1399*, 8–17. [[CrossRef](#)]
57. Li, S.; Lu, C.; Zhu, F.; Jiang, R.; Ouyang, G. Preparation of C₁₈ composite solid-phase microextraction fiber and its application to the determination of organochlorine pesticides in water samples. *Anal. Chim. Acta* **2015**, *873*, 57–62. [[CrossRef](#)]

Disclaimer/Publisher's Note: The statements, opinions and data contained in all publications are solely those of the individual author(s) and contributor(s) and not of MDPI and/or the editor(s). MDPI and/or the editor(s) disclaim responsibility for any injury to people or property resulting from any ideas, methods, instructions or products referred to in the content.